Melt blending and characterization of carbon nanoparticles-filled thermoplastic polyurethane elastomers

Sílvia M. Cruz and Júlio C. Viana

Abstract

In this work, thermoplastic polyurethane (TPU) elastomers reinforced with carbon nanosized particles were produced by a special melt blending technique. A TPU was melt blended with high-structured carbon black and carbon nanofibres (1 wt%). A miniature asymmetric batch mixer, which applies high shear levels to the melt, ensured good particles dispersion. The TPU material systems were then thoroughly characterized using thermogravimetric analysis, differential scanning calorimetry, tensile mechanical testing, electrical resistance measurements and flammability tests. The different nanofillers exhibited different influences on the TPU properties, these materials featuring interesting and improved multifunctional behaviours, with high propensity for large deformation sensors applications.

Introduction

The outstanding properties resulting from the incorporation of carbon nanofillers into polymeric matrices (nanocomposites) have generated a high scientific and technical interest in their research and study. It has been a long time since carbon particles were

Institute for Polymers and Composites (IPC)/I3N, University of Minho, Campus de Azurém, Guimarães, Portugal

Corresponding author:
Júlio C. Viana, Institute for Polymers and Composites (IPC)/I3N, University of Minho, Campus de Azurém, Guimarães 4800058, Portugal.
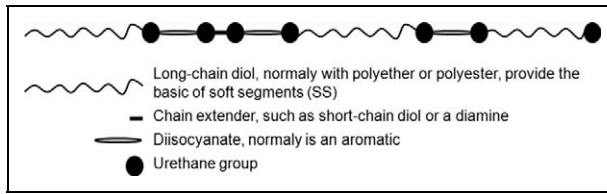Email: jcv@dep.uminho.pt

Figure 1. Schematic representation of a segmented TPU copolymer. TPU: thermoplastic polyurethane.

introduced into polymers in the engineering practice (e.g. tyres). More recently, researchers have reported[1–3] that the addition of carbon nanoparticles allows an adjustment in the properties of polymers, making them a more advantageous and versatile class of materials with extraordinary economical potential. In particular, the study of carbon nanofilled thermoplastic polyurethane elastomers (TPU) have shown enhancements upon their mechanical,[2] electrical[4] and thermal performance,[5,6] maintaining the processability and deformability characteristics of the polymer matrix. In spite of this, within the reported work, the characterization (mainly morphological) of nanoparticles-reinforced TPU is scarce.

TPUs are a class of block copolymers that consist of soft rubber segments (conferring their elastic character) and hard glassy or crystallizable chain segments (acting as physical cross-link bonds and imparting stiffness and strength).[7,8] Under service, TPUs behave as elastomers and, in contrast to the classical elastomers, they can be processed by means of the conventional techniques and equipment used for common thermoplastics. The peculiarity of TPU is related to the different nature of cross-linkings in their structure. One of the monomers develops the hard, or crystalline, regions that function as a thermally stable component (which softens and flows under shear, as opposed to the chemical cross-links between polymeric chains in a conventional thermosetting rubber); the other monomer develops the soft or amorphous regions, which contribute to its rubbery characteristic nature (Figure 1).

A key attribute of most TPU is the possibility of tailoring toughness and large strain elasticity by varying the type of monomers, the ratio of hard/soft fractions and the lengths of the hard segments (HS) and soft segments (SS).[9] Therefore, TPU has been often used in engineering applications requiring high toughness and large strain elasticity, as required in automotive and footwear applications, where conventional elastomers cannot provide the range of physical properties needed for the products. TPUs are a subcategory of the thermoplastic elastomers (TPE) and have become a target of great interest in the past decade[10–13] due to their mechanical properties (high elongation at break, high strength, good abrasion resistance and high modulus) compared to other elastomers.

Polymers have characteristically a very high electrical resistance.[14] When conductive grades are required, base polymers are modified to prevent unwanted accumulation of charge or to create conductive pathways. Part of the developed work conducted on carbon particles-filled composites is motivated, on one side, by the potential performance of

these fillers in the TPU reinforcement and, on the other side, by the unique characteristics of the resulting composite. This makes these composites attractive and of critical importance for the integration in a wide spectrum of high-performance applications, where high electrical/thermal conductivity and mechanical performance are the most important final properties (e.g. polymers for electronics, aerospace structural components, military components, medical devices[5,15] energy storage and energy conversion devices, sensors, field-emission displays and radiation sources, nanometer-sized semiconductor devices, probes and interconnects etc).[16]

In the last few years, some systematic studies of the thermophysical[17] and electrical properties[3] of composites have been published. Carbon materials also have great potential to be economically important for thermal management as observed by Zhou et al.[18] The carbon nanofillers, such as high-structured carbon black (HSCB), and carbon nanofibres (CNF) are excellent candidates for multifunctional nanoreinforcement of TPUs because of their high strength, modulus, high thermal conductivity (higher than copper and silver), excellent electrical properties and thermal stability. Powers et al.[3] have evaluated CNFs as TPE-reinforcing agents. They observed that low amounts of CNF (1–5% of incorporation) led to TPU mechanical and electrical property improvements. The electrical properties of a composite (in this case a styrene–butadiene–styrene-filled with carbon black) are determined by the incorporated volume fraction of the conductive filler, structure properties, orientation in the matrix, porosity and mixing conditions as observed by Khastgir et al..[19–21] Homer et al.[17] observed that the electrical properties of a composite also depend upon the physicochemical properties of both polymer and filler (such as particle size, shape, porosity, surface area e.g. smaller and spherical particles or fibres and longer particles have different effects) as well as the composite processing conditions, such as temperature .

For a conductor-filled polymer to be electrically conductive, the fillers must either touch to form conductive paths[22] or be sufficiently close to each other to enable conductance via 'tunnelling effect', as observed by Simmons[23] and Sheng et al.[24] This is usually defined as the percolation transition, which is characterized by a sharp drop in the electrical resistivity. The critical weight or volume fraction of filler is the threshold separating the composite into insulator or conductor.[17]

The HSCB consists on relatively many prime particles of an amorphous form of carbon with a structure similar to disordered graphite,[25] forming small particles organized in microsized aggregates. The CNFs are cylindrical nanostructures with graphene layers arranged in a wide range of orientations with respect to fibre axis. However, it is difficult to disperse homogeneously such nanoparticles into a polymer matrix[26] due to their nature and the existence of synthesis-induced entangled aggregates with high van der Waals interactions between nanoparticles.[27–30] Not much has been reported in the literature about the use of melt mixing of carbon nanoparticles into TPU. This reveals a challenging task to obtain a properly dispersion of carbon particles in TPU matrices in order to achieve the full potential of nanocomposites with improved properties and multifuncionalities. To disperse nanoreinforcements, melt mixing methods are usually preferred due to the versatility of the production facilities,[31] the reduced environmental impact of the technology and the compatibility with current industrial processes.[27–29]

In order to incorporate these materials into a new polymer material system, laboratory scale melt mixing devices are essential. It is necessary for the mixer to be capable of dealing with tiny amounts of materials, to apply enough energy and power to exert the required mechanical mixing loading, to have the flow patterns essential for obtaining homogeneous dispersion and uniform structures and to be representative of the flow encountered in industrial scale equipment.

This work has been undertaken to study the properties of nanofilled TPU with improved properties with a very small incorporation of reinforcing fillers, in order to minimize its negative impact on the processability, deformability and surface finish of the final composite system. For comparison, two types of carbon nanofillers were used. The focus of the study is on the characterization of the morphology of developed TPU nanocomposites and their electrical, mechanical, thermal and flame resistance properties, probing their advantageous multifunctional behaviour.

Experimental

Materials

This experimental work was conducted using two different types of nanoparticles:

- HSCB particles PRINTEX® XE 2 with 30 nm particle size, 0.13 g cm^{-3} of density and 910 m^2 g^{-1} surface area were obtained from from Degussa AG (Germany);
- A polymer-based dust-free nanofibre masterbatch from Electrovac with 20% of CNF incorporated (CNF with 80–150 nm diameter range and 20–100 m^2 g^{-1} specific surface area).

These particles were mixed with an amorphous-semicrystalline TPU (polyester based), AVALON 65 AE from Huntsman (Salt Lake City, Utah, USA) with a melt flow index of 21.30 g/10 s (200°C; 2.16 kg) according to ASTM D 1238-04 standard (65 Shore A of hardness and 1.18 g cm^{-3} of density).

Samples preparation

The composite TPU/nanoparticles systems were prepared by melt blending using an ultrahigh shear laboratory-scale miniature mixer (Figure 2(a)) similar to the method proposed by Breuer.[32]

The mixer design consists of a rotor with a unique asymmetric shape, spinning at high velocity (hundreds of revolutions per minute) within a heated cup (Figure 2(b)). This rotor has a length of 50 mm. The cup has an inner diameter of 26 mm and a height of 48 mm. The clearance between the tips of the rotor and the cup wall enable the material to be iteratively squeezed and stretched at high shear. A heating band is placed around the mixer and a thermocouple is inserted in the outer cup for temperature measurement and control, so that a steady temperature can be maintained. In this study, grinded TPU was previously dried at 100°C for 2 h. The TPU nanocomposites systems were prepared using a total of 20 g per sample and 1 wt% of particles. Melt blending was performed at
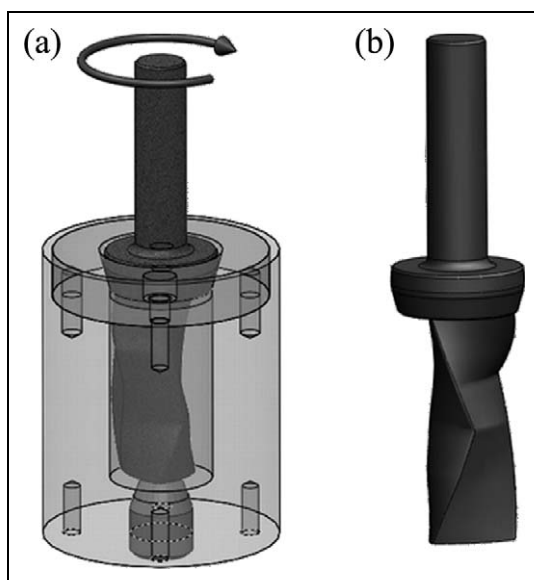
Figure 2. Design scheme of miniature mixer device. (a) Assembly and (b) cylindrical rotor.

190°C and 220 r min^{-1} for 3 min. The blended TPU was discharged on a metallic mould spacer with dimensions of $145 \times 106 \times 0.7$ mm^3 and then sandwiched between two stainless steel plates covered with Teflon foil at a pressure of 774 MPa. This procedure takes 5 min in order to ensure that the plaques would be free of air bubbles and with a uniform 0.7 mm thickness. Afterwards, the plaques were quenched in water at room temperature (23°C). The pure TPU and the two composite systems specimens were kept in a controlled temperature room (23°C) for at least 3 weeks before performing any experimental test according to ASTM D618-00 standard.

Morphological characterization

Scanning electron microscopy. The nanocomposites morphology, the fillers dispersion, agglomeration and the adhesion between the nanofillers and the TPU were observed using a scanning electron microscopy (SEM), in a Leica/Cambridge S360 electronic microscope, Cambridge, UK, under an operation voltage of 10–15 kV. Cross-sections of the composites were prepared by fracturing the TPU composites in liquid nitrogen to produce an intact fractured surface morphology. In order to avoid electrostatic charging, the fractured surface specimens were previous gold coated (sputter coater SC502, Fisons Instruments, UK).

Properties characterization

Mechanical characterization. Tensile test specimens were cut in the shape of dog bone ($50 \times 8 \times 4$ mm^3 with 0.7 mm thickness) from the compression-moulded plates. The

mechanical tests were conducted according to the ISO527-2:1993 standard. Tests were performed in a universal testing machine, Instron 4505 (Norwood, Massachusetts, USA), in a controlled environment (at 23°C and 55% relative humidity (RH)), at a crosshead velocity of 10 mm min^{-1} (corresponding to a nominal strain rate of 6.7×10^{-1} s^{-1}) until break. Engineering stress was calculated as $\sigma = F/A_0$, where F is the force and A_0 is initial specimen cross section. The engineering strain was determined by $\varepsilon = \Delta L/L_0$, where ΔL is grip displacement and L_0 is the initial reference length. From the stress–strain curves, several point properties were calculated. E_1 is the secant modulus at 1% strain and modulus 2 (E_2) and modulus 3 (E_3) were determined by the tangent method (see Figure 9 for graphical representation). The yield stress (σ_y) and strain (ε_y) were assessed by the intersection of the stress–strain curve with a line parallel to the initial slope of the curve with the tangent to curve in the initial deformation zone also used to determine E_2. The stress (σ_b) and strain at break (ε_b) were obtained directly from the measured curves. At least six specimens per measurement were used. After tensile tests, the deformed area of the specimens was also observed using SEM.

Thermal characterization

Thermogravimetric analysis. Thermogravimetric analysis (TGA) was performed under nitrogen atmosphere using a thermogravimetric analyzer (model Q500; TA Instruments, New Castle, Delaware, USA). The sample was heated from 30°C to 800°C at a heating rate of 5°C min^{-1}. The initial temperatures of weight loss for the first and second steps (Figure 3.) were denoted T_{d1} and T_{d2}, and the corresponding temperatures at the maximum rate of weight loss of were denoted DTG1$_{max}$ and DTG2$_{max}$, respectively.
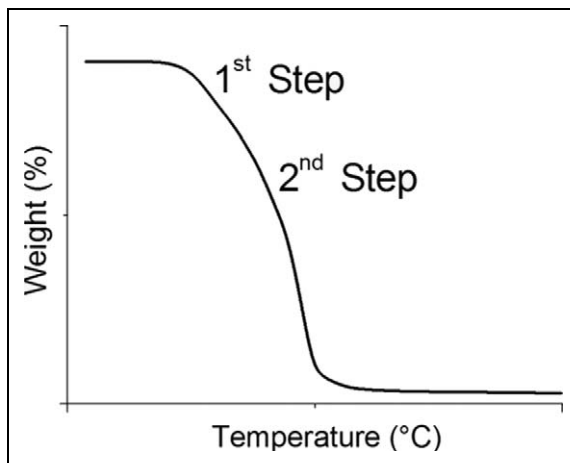

Figure 3. A two-step TGA characteristic curve of a thermal decomposition reaction. TGA: thermogravimetric analysis.

Differential scanning calorimetry. The SS glass transition temperature (T_{gSS}), the HS glass transition temperature (T_{gHS}), the HS melting point (T_{mHS}) and respective melting enthalpies of the neat and TPU composites were determined using differential scanning calorimetry (DSC) using a DSC Q20 (TA Instruments). The DSC specimens have approximately the same weight (± 10 mg), and 40 ml aluminium pans were used. An empty pan was used as the reference. The test began with an initial temperature of $-80°CC$ up to $200°CC$, at a heating rate of $20°C$ min^{-1} under nitrogen atmosphere (first heating). Then, the samples were cooled down to $-80°C$ (cooling) and reheated at the same rate to $200°C$ (second heating).

Electrical characterization

Surface and volume resistivity measurements were performed using the two-point contact method, at $23 \pm 2°C$ and $50 \pm 5\%$ of RH. The surfaces of the specimens were cleaned according to ISO 3915:1981 standard. Afterwards, chemical vapour deposition was used to create two golden layers with glued copper wires, thus ensuring a good electrical contact. For the surface measurements configuration, the electrodes have 6×2 mm length and 1 mm distance apart (Figure 4(a).). For volume measurements configuration, the electrodes have 2.5 mm radius (Figure 4(b)) and 0.75 mm distance (sample thickness).

A constant voltage was applied, and an automated Keithley 487 picoammeter (Cleveland, Ohio, USA)/voltage source was used to measure the low currents. The voltage was varied and the current intensity measured, being obtained intensity-applied voltage plots, I-V. The resistance, R, was calculated through the slope of I-V curves, with Ohm's law: $R = \frac{V}{I_e}$, where V is the applied voltage and I_e is the current flowing through the specimen. The surface resistivity (ρ_s) was calculated by:

$$\rho_s = \frac{RW}{d} \qquad (1)$$

where W is the width of the electrodes and d is the distance between them. The volume resistivity (ρ_v) was calculated by:
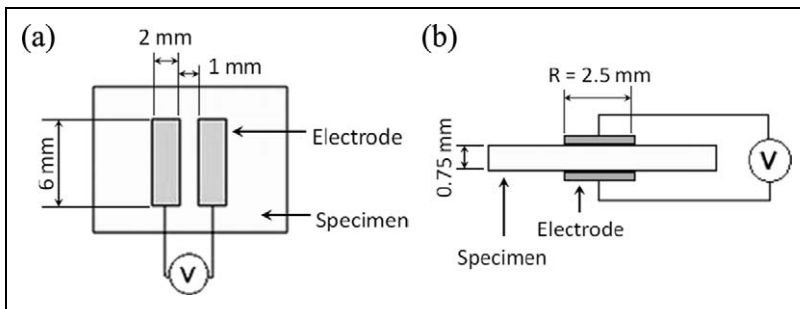

Figure 4. Electrical measurements (a) surface electrode configuration and (b) volume electrode configuration.

$$\rho_v = \frac{RA}{d} \tag{2}$$

where R is the bulk resistance, A is the cross-sectional area of specimen and d is the fixed distance between measuring points of the probes.[33–36]

Flammability tests

To evaluate the effect of reinforcing fillers on the burning properties, the specimens were tested in a horizontal burn according to ASTM D 635-03 standard. The method consists on measuring the burning rate in a horizontal position, when subjected to a pilot flame. The burning rate, in millimetre per minute, between reference lengths of 25 and 100 mm was measured. Tests were conducted at 23°C and 50% RH. The dimensions of the specimens were length = 125 mm; breadth = 13 mm; diameter = ±0.7 mm. The results are intended to serve as a preliminary indication of their acceptability with respect to flammability for a particular application. The linear burning rate (V_b) for each specimen, where the flame front reaches the 100 mm reference mark, was calculated by $V_b = 60L/t$, where L is the burned length and t is the time.

Results and discussion

Dispersion of the nanofillers in the TPU matrix

The nanocomposites morphology was observed by SEM in order to evaluate the dispersion level of the nanofillers and its adhesion to the polymer matrix. SEM images showed that the adopted mixing procedure induces a good dispersion of the nanofillers in the TPU matrices. The HSBC particles are very small and fairly well distributed (Figure 5(a)).

Occasionally, agglomerates of HSCB particles with 90 nm size were detected. The size variation of the HSCB particles reveals that the input process energy was not capable of breaking all the HSCB aggregates, but well dispersed small particles were
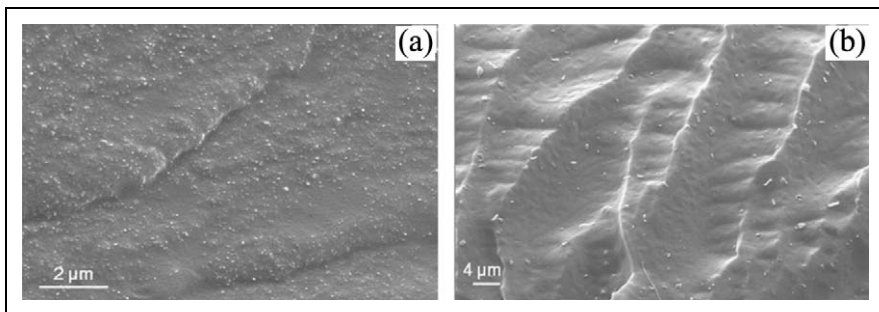

Figure 5. SEM-fractured surface images of (a) TPU + HSCB and (b) TPU + CNF. SEM: scanning electron microscopy; TPU: thermoplastic polyurethane; HSCB: high-structured carbon black.

obtained. Figure 5(b) shows a uniform dispersion of the CNF in the TPU matrix, with absence of agglomerates. Measured nanofibres diameters are between 120 and 400 nm, much higher than the average diameter of 80–150 nm indicated by the supplier. This higher diameter suggests that some polymer covers the nanofibre surface, indicating good interaction at the fibre polymer interface resulting in a good adhesion between the polymer and the CNF. The adhesion between the nanofillers and the polymer matrix is fairly good, with no voids and no particle decohesion seen in the SEM images.

DSC analysis

DSC was used to investigate the thermal transitions on heating and cooling of neat and filled TPU composites. The presence of fillers could not only modify the T_g but also could interfere on the melting and crystallization processes. DSC traces of the first melting and cooling sweeps of neat and TPUs composites are shown in Figure 6. The thermal parameters are listed in the Table 1.

These curves show two glass transitions at around -48 and $60°C$ attributed to the T_g of T_{gSS} and T_{mHS}, respectively, and a very small and broad melting peak centred at $140–150°C$, corresponding to T_{mHS}. The amorphous soft phase of the filled TPU shows a T_{gSS} around $-48°C$, which is close to the T_{gSS} of the pure TPU, indicating the absence of interactions between the nanofillers and the SS phases. The effect of addition of HSCB and CNF on the TPU is clearly seen on T_{gHS} and T_{mHS}. The incorporation of the fillers increased the HS's T_{mHS} and the melting enthalpy (ΔH_{mHS}), which may reflect bigger HS domains (rich phase) and an increment upon their degree of crystallinity. CNF particles have the highest effect on the TPU thermal transitions.

DSC traces of the second melting sweep (after erasing the processing history) of the neat TPU and its composites are shown in Figure 7. DSC data are listed in Table 2.

For neat and filled TPU, T_{gSS} is around $-43°C$, slightly lower than in the first scan, so no major changes in the T_{gSS} were registered. The effect of the nanoparticles incorporation into the TPU is clearly seen on the increment of T_{mHS} and ΔH_{mHS}. Once again,
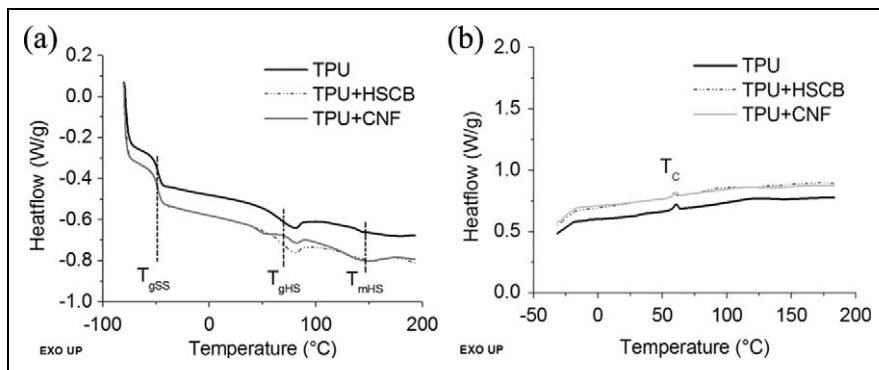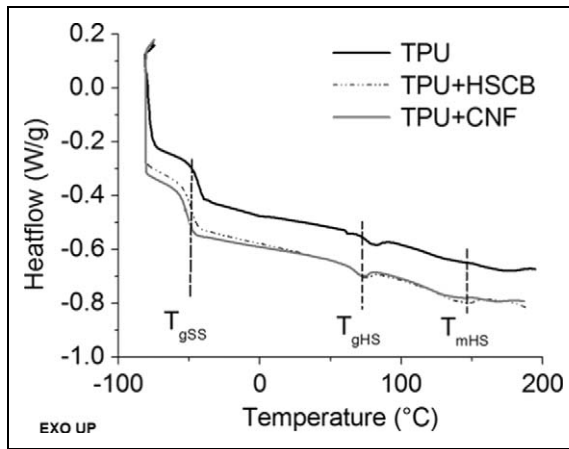

Figure 6. Thermal transitions of neat and nanofilled TPU at (a) first melting sweep and (b) cooling sweep. TPU: thermoplastic polyurethane.

Table 1. Main thermal transitions of neat and nanofilled TPU (first melting and cooling sweep).

Sample	T_{gSS} (°C)	T_{gHS} (°C)	T_{mHS} (°C)	ΔH_{mHS} (J g^{-1})	T_C (°C)	ΔH_C (J g^{-1})
TPU	−48.02	66.20	143.65	0.22	60.59	0.63
TPU + HSCB	−47.47	63.09	153.54	2.16	59.38	0.30
TPU + CNF	−48.04	76.70	152.64	3.48	60.65	0.45

TPU: thermoplastic polyurethane; HSCB: high-structured carbon black; CNF: carbon nanofibre; T_{gSS}: soft segment glass transition temperature; T_{gHS}: hard segment glass transition temperature; T_{mHS}: hard segment melting point; ΔH_{mHS}: hard segment melting enthalpy; T_C: crystalline temperature; ΔH_C: crystalline enthalpy.

Figure 7. Thermal transitions of neat and nanofilled TPU (second melting sweep). TPU: thermoplastic polyurethane.

the addition of CNF shows a remarkable enhancement of the thermal properties, interacting with the TPUs' HS domains. Furthermore, for the TPU composites, the first sweep evidences stronger thermal transitions as compared to the second sweep, revealing a significant effect of the processing thermomechanical conditions on the developed morphology.

Table 2. Main thermal transitions of neat and nanofilled TPU (second melting sweep).

Sample	T_{gSS} (°C)	T_{gHS} (°C)	T_{mHS} (°C)	ΔH_{mHS} (J g^{-1})
TPU	−43.12	77.12	143.37	0.25
TPU + HSCB	−42.71	76.53	145.78	1.96
TPU + CNF	−43.30	76.13	149.72	1.30

TPU: thermoplastic polyurethane; HSCB: high-structured carbon black; CNF: carbon nanofibre; T_{gSS}: soft segment glass transition temperature; T_{gHS}: hard segment glass transition temperature; T_{mHS}: hard segment melting point; ΔH_{mHS}: hard segment melting enthalpy.

Thermogravimetric analysis

The effect of the reinforced particles on the thermal stability of TPU was evaluated by TGA. The mass loss variations with temperature for neat and reinforced TPUs are shown in Figure 8.

No expressive weight loss was registered between 30°C and 200°C. The first degradation process corresponds to the release of the little molecules or unstable side chains, which will degrade at lower temperature.[37] Thermal degradation of TPUs is an intricate process. It has been found that the thermal degradation of TPUs occurs in two stages,[38,39] since HS and SS respond differently at high temperatures. In the first step, decomposition of the HS occurs, involving dissociation of urethane from the original polyol and isocyanate. In the second step, condensation and polyol degradation of the SS take place. Therefore, first stage can be associated with T_{d1} of HS, whilst the second stage can be related to T_{d2} of SS.[39–41] Table 3 shows the thermal stability improvement of the TPU nanocomposites. The first degradation of the neat TPU occurred at 192°C and the second degradation at 342°C. As it can be noticed, both HSCB and CNF appear to affect differently TPUs hard and soft domains degradation.

The incorporation of the HSCB did not change T_{d1} significantly (approximately 3°C), but improved T_{d2}, delaying it by approximately 12°C. The CNF presence delayed slightly the first degradation temperature by approximately 4°C, whilst T_{d2} is reduced by approximately 34°C. During degradation, the nanoparticles interact preferably with the SS in polyurethane structure. Also, these results suggest that the CNF interacted more with HS and SS domains than HSCB particles. Expectantly, the thermal stability is improved with the incorporation of more thermally stable fillers such as the HSCB and the CNF, as already reported elsewhere.[42] This was interpreted by the adsorption of free radicals by the carbon fillers surface[39], the uniformly dispersed carbon nanofillers presumably providing higher thermo-oxidative stability to the polymers in the vicinity of
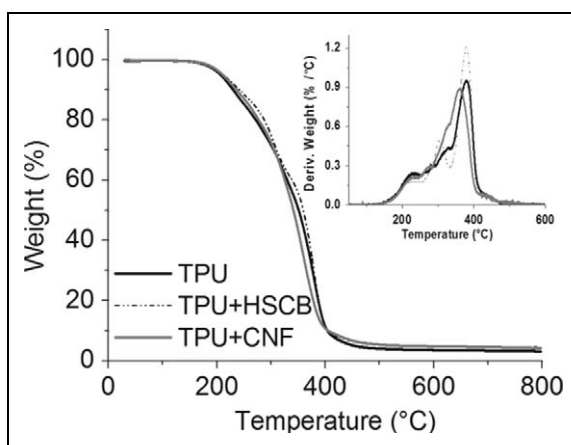

Figure 8. Weight loss from TGA analysis under N_2 atmosphere of neat and nanofilled TPU. TGA: thermogravimetric analysis; N_2: nitrogen; TPU: thermoplastic polyurethane.

Table 3. TGA results of neat and nanofilled TPU.

	T_{d1} (°C)	$DTG1_{max}$ (°C)	T_{d2} (°C)	$DTG2_{max}$ (°C)
TPU	191.82	229.73	342.13	380.04
TPU + HSCB	188.78	218.68	354.25	379.82
TPU + CNF	195.71	222.09	307.67	361.52

TPU: thermoplastic polyurethane; HSCB: high-structured carbon black; CNF: carbon nanofibre; T_{d1}: initial weight loss temperature for the first step; T_{d2}: initial weight loss temperature for the second step; $DTG1_{max}$: temperature at the maximum rate of weight loss for the first step; $DTG2_{max}$: temperature at the maximum rate of weight loss for the second step.

the fillers surfaces[43] and the enhancement of the thermal conductivity of the composite that can facilitate heat transport and thus increase its thermal stability.[44]

Mechanical properties analysis

The effect of the type of filler on the composites' mechanical properties was analyzed. For each TPU system, a representative curve was selected and plotted for comparison as depicted in Figure 9. The two composite systems show similar behaviour, but with much higher deformation and stress levels as compared to the unreinforced TPU. These results clearly reveal that the added nanosized particles increased dramatically the TPUs mechanical properties. Table 4 shows the mechanical properties of the neat and nano-filled TPU.

The nanocomposites have higher modulus (TPU + CNF) and superior strength (mainly at break) when compared with the neat TPU. The highest modulus, E_1, of the TPU + CNF nanocomposites reflects the good adhesion of the CNF to the TPU matrix
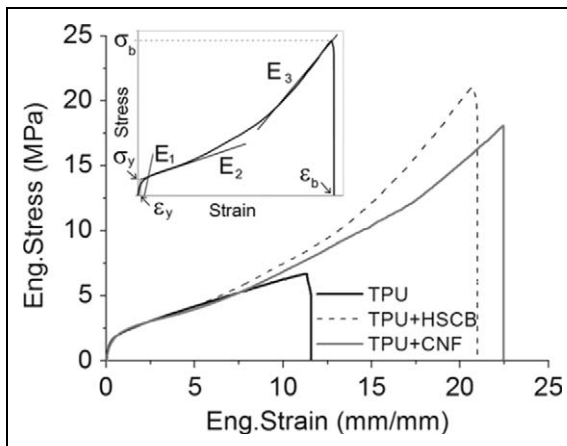

Figure 9. Engineering stress–strain curves of neat and nanofilled TPU (inset graph). TPU: thermoplastic polyurethane.

Table 4. Mechanical properties of neat and nanofilled TPU.

Sample	E_1 (MPa)	E_2 (MPa)	E_3(MPa)	σ_y (MPa)	ε_y	σ_b (MPa)	ε_b
TPU	13.36 ± 3.30	0.45 ± 0.03	0 ± 0.00	2.10 ± 0.19	0.65 ± 0.05	7.44 ± 1.20	13.16 ± 2.32
TPU + HSCB	8.61 ± 3.07	0.78 ± 0.05	1.18 ± 0.47	2.34 ± 0.05	1.05 ± 0.21	21.75 ± 1.14	21.39 ± 0.60
TPU + CNF	38.10 ± 1.20	0.75 ± 0.03	1.15 ± 0.16	2.29 ± 0.04	1.00 ± 0.06	20.69 ± 2.36	23.26 ± 0.72

TPU: thermoplastic polyurethane; HSCB: high-structured carbon black; CNF: carbon nanofibre; E_1: secant modulus at 1% strain; E_2: tangent modulus at 2% strain; E_3: tangent modulus at 3% strain; σ_y: yield stress; ε_y: yield strain; σ_b: stress at break; ε_b: strain at break.

that allows a larger contribution of the stiffer particles to the modulus. Also, the higher interfacial area and aspect ratio of the CNF allows the formation of a kind of a more rigid network that withstands the initial deformations. All nanocomposites sustain very high stress and strain levels when compared with the neat TPU. This enhancement on the mechanical properties is thought to be associated with:

- a good nanofiller adhesion to the TPU matrix, resulting in higher modulus and strength;
- the increased number of molecular entangled regions that allow sustaining higher stress levels and
- the progressive disentanglement and easier sliding of macromolecules allowing a high deformation capability.

Further evidence of the significant mechanical behaviour improvement of TPU composites is provided by the SEM images of deformed specimens, as illustrated in Figure 10. Figure 10(a) shows a massive local matrix deformation of TPU filled with HSCB. This appears to be originated by the well-dispersed HSCB nanofillers.

In Figure 10(b), it is evident that the nanofibres have a good adhesion to the polymeric matrix, showing no voids at the interface with the TPU, even for the high deformation levels. Furthermore, the nanofibres are highly oriented in the stretching direction. This is extremely interesting, being evidenced, besides the strong adhesion of the nanofibre to the TPU matrix, that the CNFs are forced to align on the stretching direction by the external stress field.

Electrical resistivity measurements

The variations of the surface and volume electrical resistivity measurements with the different nanofillers incorporation is shown in the Table 5.

As expected, the incorporation of the conductive fillers decreases the electrical resistivity of the composites, mainly for the CNFs that reduce surface resistivity by two orders of magnitude (just for 1 wt% of incorporation). The variations of the volume
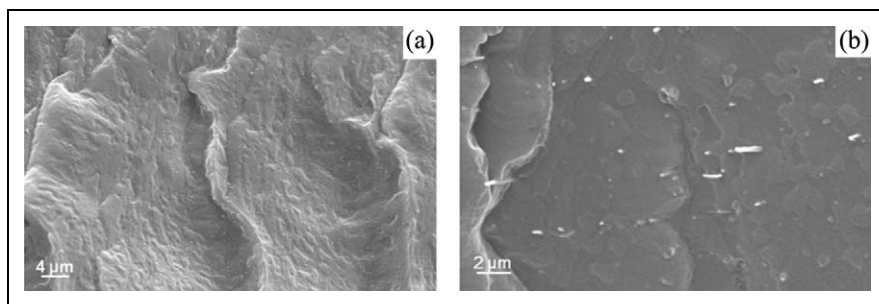

Figure 10. SEM-fractured surface images of specimens after tensile tests in (a) TPU + HSCB and b)TPU + CNF. SEM: scanning electron microscopy; TPU: thermoplastic polyurethane; HSCB: high-structured carbon black; CNF: carbon nanofibre.

Table 5. Surface and volume electrical resistivity measurements results of neat and nanofilled TPU.

	TPU	TPU + HSCB	TPU + CNF
Surface resistivity (Ω)	5.00E + 11	1.20E + 11	6.00E + 09
Volume resistivity (Ω cm)	3.00E + 16	7.85E + 10	2.09E + 09

TPU: thermoplastic polyurethane; HSCB: high-structured carbon black; CNF: carbon nanofibre.

Table 6. V_b results of neat and nanofilled TPU.

Sample	Thickness (mm)	V_b (mm/min^{-1}))
TPU	0.50	79.21 $\pm$ 15.26
TPU + HSCB	0.56	62.50 $\pm$ 17.68
TPU + CNF	0.56	73.90 $\pm$ 33.80

V_b: linear burning rate; TPU: thermoplastic polyurethane; HSCB: high-structured carbon black; CNF: carbon nanofibre.

resistivity are much higher, being reduced by six and seven orders of magnitudes for reinforcement with the HSCB and the CNF, respectively. In conductive composites, aggregated and agglomerated phases can form a conductive three-dimensional network of conductive particles through the system, and electrical conductivity is achieved. As shown in the SEM images of the HSCB and the CNF composites (Figure 5(a) and (b)), these fillers have a high level of dispersion, thus reducing the decrement on the electrical properties. Although using a melt blending process and only 1 wt% of incorporation of conductive nanoparticles, the studied nanocomposites achieved a significant drop in their electrical resistivity, mainly for the case of the CNF-reinforced TPU. It is expected that an increment upon the amount of incorporation will reduce further the electrical resistivity. The smaller drop on the surface resistivity as compared to the higher reduction on the volume resistivity suggests that a superficial layer rich of insulated TPU is developed. This layer is formed due to the lower viscosity of neat TPU that promotes filler segregation during samples manufacturing and the flow of the low viscosity matrix into the surface of the compression-moulded plates.

Flame resistance

Numerous studies have shown that the introduction of nanoparticles into polymers can greatly improve their properties such as flame resistance, reducing the heat released and improving fire retardancy.[42] Table 6 shows the variations of V_b with filler addition for both composite systems.

The addition of HSCB decreased greatly the TPU's V_b. This enhancement is thought to be associated with the creation of carbon barrier that delays the combustion. Interestingly, the incorporation of the CNF particles had a small effect on the flammability of the TPU. It has been observed that at low carbon contents (1 wt%), the thermal stability

of the nanofilled TPU is facilitated; this property is attributed to the enhancement of thermal conductivity of the TPU composite.[45] For higher levels of incorporation, the thermal stability is improved (thermal degradation is delayed).

Conclusion

The blending procedure adopted in this work makes possible to obtain well-dispersed conductive nanofillers in a TPU matrix. A good adhesion between the TPU and the nano-fillers was evidenced. Well-dispersed fillers provided larger contact surface and a strong interfacial interaction between the filler and the polymer matrix, avoiding local stress concentrations, which is translated in an enhancement on the TPU nanocomposites mechanical properties. The incorporation of such fillers strongly influence the polymer chain mobility, clearly revealing improvements in the modulus, sustained stress level and strain at break, especially for the CNF fillers. Different types of nanoparticles exhibit distinct influences on the properties of the nanofilled TPU.

The incorporation of the nanoparticles had a great effect on the crystallization of the TPU nanocomposites. T_{mHS} and ΔH_{mHS} increase significanty, reflecting bigger HS domains and an increment upon their degree of crystallinity. The nanoparticles interact strongly with the HSs of the TPU, their T_{gHS} and T_{mHS}. Conversely, there is an absence of interactions with the SS. CNFs have the highest effect on the TPU thermal transitions. The effect of processing thermomechanical conditions on the developed morphology of the TPU is rather important.

The thermal degradation of the TPU occurs in two stages, which can be related to the response of the HS and SS. Both nanofillers appear to affect differently TPUs hard and soft domains degradation. During thermal degradation, the nanoparticles interact pre-ferably with the SS and more strongly for the CNF-filled TPU. The thermal stability of the nanocomposites is improved significantly.

A small drop in electrical resistance was observed when compared with pure TPU, but clearly the percolation limit was not reached for 1 wt% of incorporation of the nanofillers. The reductions on the volume resistivity are higher (six to seven orders of magnitude) than the surface resistivity (only two orders of magnitude), suggesting the formation of a superficial layer rich on neat TPU that was formed during the plates manufacturing process. The variations on the electrical resistivity are higher for the CNF-filled TPUs.

The incorporation of the HSCB into the TPU also led to a major decrement upon flammability of the samples. This was associated with the creation of carbon barrier that delays the combustion. But, for the case of incorporation of CNF particles, the flammability has only diminished slightly, which was attributed to the enhancement of the thermal conductivity of the composite TPU.

This work also evidenced that the incorporation of carbon-based nanofillers results in a mulfunctional behaviour of the TPU, with a concomitant and significant improvements on their mechanical, thermal, electrical and flame resistance behaviour, without compro-mising its deformability. These thermoplastic elastomers reinforced with nanosized par-ticles show improved performance and added functionalities that make then promising materials for several applications.

Acknowledgements

Funding

References

1. Das A, Stöckelhuber KW, Jurk R, et al. Modified and unmodified multiwalled carbon nanotubes in high performance solution-styrene-butadiene and butadiene rubber blends. *Polymer* 2008; 49: 5276.
2. Koerner H, Liu W, Alexander M, et al. Deformation-morphology correlations in electrically conductive carbon nanotube–thermoplastic polyurethane nanocomposites. *Polymer* 2005; 46: 4405.
3. Powers DS, Vaia RA, Koerner H, et al. NMR Characterization of low hard segment thermoplastic polyurethane/carbon nanofiber composites. *Macromolecules* 2008; 41: 4290.
4. In K. Investigation of electrically conductive acrylonitrile-butadiene rubber. *J Vinyl Add Tech* 2007; 13: 71.
5. Biercuk MJ, Llaguno MC, Radosavljevic M, et al. Carbon nanotube composites for thermal management. *Appl Phys Lett* 2002; 80: 2767.
6. Golecki I, Xue L, Dewar DM, et al. Properties of high thermal conductivity carbon-carbon composites for thermal management applications. In: *IEEE conference on devices and sensors*, San Diego, CA, 22–27 Feb. 1999.
7. Fakirov S (ed). *Handbook of Condensation Thermoplastic Elastomer*. 1st ed. Germany: WILEY-VCH Verlag, 2005.
8. Holden G, Legge NR, Quirk RP, et al. *Thermoplastic Elastomers*. 2nd ed. New York, NY: Hanser, 1996.
9. Honeker CC and Thomas EL. Impact of morphological orientation in determining mechanical properties in triblock copolymer systems. *Chem Mater* 1996; 8: 1702.
10. Dutta NK, Bhowmick AK and Choudhury NR. In: Olagoke O (ed) *Handbook of Thermoplastic Elastomers*. New York, NY: Marcel Dekker, 1997, Chapter 15: Thermoplastic Elastomers.
11. School RJ. In: Walker BM and Rader CP (eds) *Handbook of Thermoplastic Elastomers*, New York, NY: Van Nostrand Reinhold, 1988, Chapter 9.
12. Kear K.E. Developments in 'thermoplastic elastomers', *Report, Rapra Review Reports*, 2003.
13. Martin DJ, Osman AF, Andriani Y, et al. Thermoplastic polyurethane (TPU)-based polymer nanocomposites, *In: Gao F (ed) Advances in polymer nanocomposites : types and applications*, Sawston, Cambridge: Woodhead Publ., 2012, Chaper 11.
14. Knite M, Teteris V, Aulika I, et al. Alternating-Current Properties of Elastomer-Carbon Nanocomposites. *Adv Eng Mat* 2004; 6: 746.
15. Benedict LX, Crespi VH, Louie SG, et al. Static conductivity and superconductivity of carbon nanotubes: relations between tubes and sheets. *Phys Rev B* 1995; 52: 14935.
16. Lau KT and Hui D. The revolutionary creation of new advanced materials carbon nanotube composites. *Compos B* 2002; 33: 263.

17. Homer ML, Lim JR, Manatt K, et al. Temperature effects on polymer-carbon composite sensors: Evaluating the role of polymer molecular weight and carbon loading in sensors. *In: Proceeding of IEEE conference, Sensors* 2003, NASA-JPL Pub., Pasadena, Vol. 2, 22 -24 Oct 2003, p. 877.
18. Zhou Y, Jeelani S and Eranezhuth B. Improvement in thermal, mechanical and electric properties of multi-wall carbon nanotube reinforced epoxy and carbon/epoxy composite. *eXPRESS Polym Lett* 2008; 2: 40.
19. Sau KP, Chaki TK and Khastgir D. The change in conductivity of a rubber-carbon black composite subjected to different modes of pre-strain. *Compos A Ed Appl Sci Manuf* 1998; 29: 363.
20. Leyva ME, Barra GMO, Moreira ACF, et al. Electric, dielectric, and dynamic mechanical behavior of carbon black/styrene-butadiene-styrene composites. *Polym Sci B Ed Polym Phys* 2003; 41: 2983.
21. Mohanraj GT, Chaki TK, Chakraborty A, et al. Effect of some service conditions on the electrical resistivity of conductive styrene-butadiene rubber-carbon black composites. *J Appl Polym Sci* 2004; 92: 2179.
22. Vu YT, Mark JE, Pham LH, et al. Clay nanolayer reinforcement f cis-1.4- polyisoprene and epoxidized natural rubber. *J Appl Polym Sci* 2001; 82: 139.
23. Simmons GJ. Generalized formula for electric tunnel effect between similar electrodes separated by a thin insulating film. *J Appl Phys* 1963; 34: 1793.
24. Sheng P, Sichel EK and Gittleman JL. Fluctuation-induced tunneling conduction in carbon-polyvinylchloride composite. *Phys Rev Lett* 1978; 40: 1197–1200.
25. Jan-Chan H. Carbon black filled conducting polymers and polymer blends. *Adv Polym Technol* 2002; 21: 299.
26. Lai SM, Wang CK and Shen HF. Properties and preparation of thermoplastic polyurethane/silica hybrid using sol-gel process. *J Appl Polym Sci* 2005; 97: 1316.
27. Breuer O and Sundararaj U. Big returns from small fibers: a review of polymer/carbon nanotube composites. *Polym Compos* 2004; 25: 630.
28. Lin B, Sundararaj U and Guegan P. Effect of mixing protocol on compatibilized polymer blend morphology. *Polym Eng Sci* 2006; 46: 691.
29. Ray SS and Okamoto M. Polymer/layered silicate nanocomposites: a review from preparation to processing. *Prog Polym Sci* 2003; 28: 1539.
30. Potschke P, Bhattacharyya AR, Janke A, et al. Melt mixing of polycarbonate/multiwall carbon nanotubes composites. *Compos Interf* 2003; 10: 389.
31. Aso O, Eguiazábal JI and Nazábal J. The influence of surface modification on the structure and properties of a nanosilica filled thermoplastic elastomer. *Compos Sci Technol* 2007; 67: 2854.
32. Breuer O, Sundararaj U and Toogood RW. The design and performance of a new miniature mixer for specialty polymer blends and nanocomposites. *Eng Sci* 2004; 44: 5.
33. Krause B, Pötschke P and Häußler L. Influence of small scale melt mixing conditions on electrical resistivity of carbon nanotube-polyamide composites. *Compos Sci Technol* 2009; 69: 1505.
34. Ramaraj B. Polymer-plastic technology and engineering. *Taylor & Francis* 2007; 46: 575.
35. Yamaguchi K, Busfield JJC and Thomas AG. Electrical and mechanical behavior of filled elastomers. I. The effect of strain. *J Polym Sci B: Polym Phys* 2003; 41: 2079.
36. Irving PE and Thiagarajan C. Fatigue damage characterization in carbon fibre composite materials using an electrical potential technique. *Smart Mat Struct* 1998; 4: 456.
37. Han B, Cheng A, Ji G, et al. Effect of organophilic montmorillonite on polyurethane/montmorillonite nanocomposites. *J Appl Polym Sci* 2004; 91: 2536.
38. Zoran SP, Javni I, Waddon A, et al. Structure and properties of polyurethane-silica nanocomposites. *J Appl Polym Sci* 2000; 76: 133.

39. Xia H and Song M. Preparation and characterization of polyurethanecarbon nanotube composites. *Soft Matter* 2005; 1: 386.
40. Petrovic ZS, Zavargo Z, Flynn JH, et al. Thermal degradation of segmented polyurethanes. *J Appl Polym Sci* 1994; 51: 1087.
41. Chuang FS, Tsen WC and Shu YC. The effect of different siloxane chain-extenders on the thermal degradation and stability of segmented polyurethanes. *Polym Degrad Stab* 2004; 84: 69.
42. Wang ZY, Han EH and Ke W. Fire-resistant effect of nanoclay on intumescent nanocomposite coatings. *J Appl Polym Sci* 2007; 103: 1681.
43. Hwang J, Muth J and Ghosh T. Electrical and mechanical properties of carbon-black-filled, electrospun nanocomposite fiber webs. *J Appl Polym Sci* 2007; 104: 2410.
44. Huxtable ST, Cahill DG, Shenogin S, et al. Interfacial heat flow in carbon nanotube suspensions. *Nat Mater* 2003; 2: 731.
45. Jimenez GA. *Characterization of poly(methyl methacrylate) and thermoplastic polyurethane-carbon nanofiber composites produced by chaotic mixing*. PhD Thesis, University of Akron, USA, 2007.